

# From Discrete-Particle to Continuum Models

Bert Vreman

Vreman Research  
Hengelo  
The Netherlands

[www.vremanresearch.nl](http://www.vremanresearch.nl)

Material (to be) presented at the 'Advanced School on Lagrangian Techniques for Multiphase Flows' held in Trieste, Italy, 5-7 September 2007.

# 1. Introduction

## Main questions

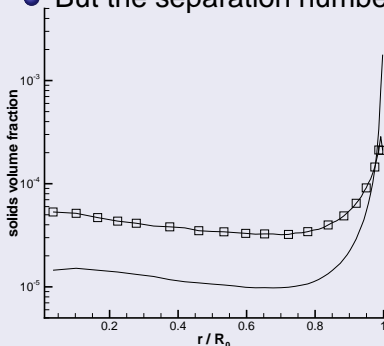
- 1 How can discrete particle models be used to validate and calibrate continuum models?
  - A discrete particle model (DPM) can be a powerful tool, but in many engineering applications there are too many particles to track individually: continuum models (CM) are still indispensable.
- 2 How can discrete particle models be used to find new physical explanations for multi-phase phenomena?

## Scope

- 1 Gas-solid flows (solid particles in a gas flow)
- 2 Regime where collisions between particles are important, so the particle volume fraction  $\alpha_s > 10^{-5}$

## Collisions are more important than generally assumed

- Standard classification (Elgobashi 1991):
  - One-way coupling: particles respond to fluid ( $\alpha_s < 10^{-6}$ )
  - Two-way coupling: fluid also responds to particles ( $10^{-6} < \alpha_s < 10^{-3}$ )
  - Four-way coupling: particles also collide ( $\alpha_s > 10^{-3}$ )
- But the separation number  $10^{-3}$  is too large! Example:



Pipe flow (Vreman 2007)

$$\alpha_s \approx 0.5 \cdot 10^{-5}$$

Concentration profiles:

(□) with collision;

(—) without collisions.

## Contents

### 1 Introduction

### 2 Computational models

- Direct Numerical Simulation (DNS)
- Euler-Lagrange approach; discrete particle models:  
hard-sphere model for dilute flows;  
soft-sphere model for dense flows.
- Continuum models: kinetic gas theory

### 3 Dilute particle-laden turbulent flows ( $\alpha_s < 0.1$ ):

- Comparison with experiments;
- Sensitivity to parameters in DPM;
- Validation of continuum models by DPM;
- New physical explanation for the turbulence attenuation in particle-laden wall-bounded flow;
- Mainly based upon: *A.W. Vreman, Turbulence characteristics of particle-laden pipe flow, J. Fluid Mech. 584, 235-279 (2007).*

## Contents (continued)

### 4 Dense granular flows ( $0.1 < \alpha_s < 0.64$ ):

- Comparison with experiments (movies);
- Validation of continuum models by DPM;
- New physical explanation for the reservoir formation in granular flow on an inclined plane through a contraction;
- Mainly based upon: *A.W. Vreman, M. Al-Tarazi, J.A.M. Kuipers, M. van Sint Annaland, O. Bokhove, Supercritical shallow granular flow through a contraction: experiment, theory and simulation, J. Fluid Mech. 278, 233-269 (2007).*

### 5 Mathematics of continuum models:

- Well-posedness of the equations (control of instabilities);
- The entropy law as guideline to construct continuum models;
- Generalization to an arbitrary number of components;
- Mainly based upon: *A.W. Vreman, Macroscopic theory of multicomponent flows: irreversibility and well-posed equations, Physica D 225, 94-111 (2007).*

# Computational models for two-phase flow

## Three computational approaches

- 1 DNS; *solves the fluid boundary layers around particles directly*; models for particle collision may be needed.
- 2 Euler-Lagrange model (DPM): gas phase is modelled with Navier-Stokes equations; solid phase with discrete particle model; *particle-gas interaction is modelled empirically* (drag law); models for particle collision.
- 3 Euler-Euler model (CM): partial differential equations for both phases; *constitutive equations needed*.

## Section contents

**2.1** Euler-Lagrange equations.

**2.3** Euler-Euler equations.

**2.2** Collision models in DPM.

**2.4** Constitutive eqs in CM.

## 2.1 Euler-Lagrange equations for small $\alpha_s$ ( $< 0.02$ )

### Mass and momentum equations

- Incompressible Navier-Stokes for gas phase:

$$\nabla \cdot \mathbf{u} = 0, \quad (1)$$

$$\rho_g \left( \frac{\partial \mathbf{u}}{\partial t} + \mathbf{u} \cdot \nabla \mathbf{u} \right) = -\nabla p + \rho_g \nu \nabla^2 \mathbf{u} + \rho_g g \mathbf{e}_z + \mathbf{a}_{ext} \mathbf{e}_z + \mathbf{f}, \quad (2)$$

- For each solid particle the Lagrangian equations:

$$\frac{d\mathbf{x}_p}{dt} = \mathbf{v}_p, \quad (3)$$

$$\rho_s V_p \frac{d\mathbf{v}_p}{dt} = \mathbf{F}_{d,p} + \mathbf{F}_{c,p} + \rho_s V_p \mathbf{g}, \quad (4)$$

## Particle gas interaction

- Drag force (Schiller & Naumann 1935)

$$\mathbf{F}_{d,p} = \frac{\rho_s V_p}{\tau_p} (1 + 0.15 Re_p^{0.687}) \left( (\mathbf{A}\mathbf{u})_p - \mathbf{v}_p \right), \quad (5)$$

$$Re_p = \frac{d_p |(\mathbf{A}\mathbf{u})_p - \mathbf{v}_p|}{\nu}, \quad (6)$$

- Source term in gas momentum equation:

$$\mathbf{f} = A^* \hat{\mathbf{f}}, \quad \hat{\mathbf{f}}(\mathbf{x}) = -\frac{1}{|W_n|} \sum_{\{p|\mathbf{x}_p \in W_n\}} \mathbf{F}_{d,p} \quad \text{if } \mathbf{x} \in W_n. \quad (7)$$

- Other forces in particle equation:

- Added mass force and gas pressure gradient force can be neglected if  $\rho_s/\rho_g$  is large (e.g. Armenio & Fiorotti 2001)
- Lift force can be important in case of large mean shear:

$$\frac{1}{2} \rho_g V_p (\mathbf{u} - \mathbf{v}) \times (\nabla \times \mathbf{u}). \quad (8)$$

## Effects of the gas volume fraction $\alpha_g = 1 - \alpha_s$

- When  $\alpha_s > 0.02$ ,  $\alpha_g$  should be included in the gas Navier-Stokes equation, like in the gas momentum equation in the continuum approaches (see later on):  $\alpha_g$  moves inside the divergence operators.
- Also the drag law should depend on  $\alpha_g$  (Ergun equation 1952 ( $\alpha_g < 0.8$ ); Wen-Yu equation 1966 ( $\alpha_g > 0.8$ ); Hill, Koch & Ladd 2001)
- Complication: gas velocity is no more divergence free (like in compressible flow).
- Particle-laden channel flow; calculations with variable  $\alpha_g$  inside the divergence operators showed that the effects of variable  $\alpha_g$  could be ignored for  $\alpha_s \approx 0.013$  (Vreman, Geurts, Deen & Kuipers 2004).

## Effects of the gas volume fraction (continued)

- For  $\alpha_s > 0.02$ , the gas equations can sometimes be neglected entirely, namely if

$$F_{collision} \gg F_{drag}. \quad (9)$$

- (9) is often valid for granular flows on inclined planes (gravity driven;  $F_{collision} \approx F_{gravity}$ ), where

$$\frac{g \sin \theta}{|v|/\tau_p} \gg 1, \quad \tau_p = \frac{\rho_s d^2}{18 \rho_g \nu_g}. \quad (10)$$

However (9) is usually not satisfied in fluidized beds and risers (drag-force driven).

## 2.2 Collision models DPM: hard- & soft-sphere

### Hard-sphere collision model

- Alder & Wainwright 1959 (elastic); Campbell & Brennen 1985 (inelastic); Hoomans et al 1996; reviews Deen et al 2006; van der Hoef et al 2006.
- The duration of a collision is infinitely short.
- Newton's second and third laws provide nine equations for twelve unknowns:

$$m_a(\mathbf{v}_a - \mathbf{v}_{a,0}) = -m_b(\mathbf{v}_b - \mathbf{v}_{b,0})(:= \mathbf{J}),$$

$$\frac{1}{5}m_a d_a(\omega_a - \omega_{a,0}) = \frac{1}{5}m_b d_b(\omega_b - \omega_{b,0}) = -\mathbf{n} \times \mathbf{J},$$

where  $\mathbf{J}$  is the impulse vector and  $\mathbf{n}$  is the unit vector directed along  $\mathbf{x}_a - \mathbf{x}_b$ .

## Hard-sphere collision model (continued)

- Three closure equations:

$$\mathbf{v}_{ab} \cdot \mathbf{n} = -e_r(\mathbf{v}_{ab,0} \cdot \mathbf{n}), \quad (11)$$

$$|\mathbf{n} \times \mathbf{J}| = -\mu_t(\mathbf{n} \cdot \mathbf{J}), \quad (\text{Coulomb}) \quad (12)$$

$$\mathbf{v}_{ab} \cdot \mathbf{t} = -\beta_0(\mathbf{v}_{ab,0} \cdot \mathbf{t}). \quad (13)$$

- Coefficients of normal restitution ( $e_r = 0.97$ ), tangential friction ( $\mu_t = 0.1$ ), tangential restitution ( $\beta_0 = 0.33$ ).
- Implementation: avoid scanning all binary pairs by using a 'collision grid' and 'neighbour lists'.

## Properties hard-sphere model:

- Very fast for dilute flows;
- Drawbacks: only binary contacts allowed; failure in dense flows (nice explanation in Goldhirsch 2003).

## Soft-sphere collision model

- Linear spring/dash-pot model (Cundall & Strack 1979; Hoomans 1999; van der Hoef, Ye et al. 2006);
- Finite interaction forces during a finite time; *expensive* since collision proces is discretized in time.
- Collision forces:

$$\mathbf{F}_{n,ab} = -\left(k_n(d - |\mathbf{r}_a - \mathbf{r}_b|) + \eta_n \mathbf{v}_{ab} \cdot \mathbf{n}_{ab}\right) \mathbf{n}_{ab} \quad \text{if } |\mathbf{r}_a - \mathbf{r}_b| < d, \quad (14)$$

$$\mathbf{F}_{t,ab} = \mu_t |\mathbf{F}_n| \quad (\text{Coulomb}). \quad (15)$$

- $\mu_t$  is the friction coefficient;  $k_n$  is the spring stiffness [N/m];  $\eta_n$  is a damping coefficient, determined by  $e_r$ .
- In fact Eq. (15) is only valid for sliding collisions; sticking collisions are more tricky. Rotation is also included.

## Soft-sphere collision model (continued)

- Equations of motion for particle  $a$ :

$$m_a \frac{d\mathbf{v}_a}{dt} = \sum_{\text{contacting } b} \mathbf{F}_{ab}, \quad (16)$$

$$\frac{d\mathbf{x}_a}{dt} = \mathbf{v}_a, \quad (17)$$

$$\frac{2}{5} m_a R_a \frac{d\omega_a}{dt} = \sum_{\text{contacting } b} R_a \mathbf{n}_{ab} \times \mathbf{F}_{ab,t}. \quad (18)$$

- Velocity difference depends on rotational velocity:

$$\mathbf{v}_{ab} = (\mathbf{v}_a - \mathbf{v}_b) + (R_a \omega_a + R_b \omega_b) \times \mathbf{n}_{ab}, \quad (19)$$

- Cohesive forces can easily be included (van der Waals forces; important for Geldart A and C particles).

## 2.3 Euler-Euler equations

### Equations for a common two fluid model

- Anderson & Jackson 1967; review van der Hoef et al 2006;
- Gas phase:

$$\frac{\partial \rho_g \alpha_g}{\partial t} + \nabla \cdot (\rho_g \alpha_g \mathbf{u}) = 0, \quad (20)$$

$$\begin{aligned} \frac{\partial \rho_g \alpha_g \mathbf{u}}{\partial t} + \nabla \cdot (\rho_g \alpha_g \mathbf{u} \mathbf{u}) &= -\alpha_g \nabla p_g + \nabla \cdot (\alpha_g \sigma) \\ &\quad -\beta(\mathbf{u} - \mathbf{v}) + \rho_g \alpha_g \mathbf{g}, \quad (21) \end{aligned}$$

## Equations two fluid model (continued)

- Solid phase:

$$\frac{\partial \rho_s \alpha_s}{\partial t} + \nabla \cdot (\rho_s \alpha_s \mathbf{v}) = 0, \quad (22)$$

$$\begin{aligned} \frac{\partial \rho_s \alpha_s \mathbf{v}}{\partial t} + \nabla \cdot (\rho_s \alpha_s \mathbf{v} \mathbf{v}) &= -\alpha_s \nabla p_g - \nabla p_s + \nabla \cdot \sigma_s \\ &\quad + \beta(\mathbf{u} - \mathbf{v}) + \rho_s \alpha_s \mathbf{g}, \end{aligned} \quad (23)$$

- Granular temperature equation  $T = \frac{1}{3}(\widetilde{\mathbf{v}} \cdot \widetilde{\mathbf{v}} - \tilde{\mathbf{v}} \cdot \tilde{\mathbf{v}})$ :

$$\begin{aligned} \frac{3}{2} \left( \frac{\partial \rho_s \alpha_s T}{\partial t} + \nabla \cdot (\rho_s \alpha_s \mathbf{v} T) \right) &= (-p_s \mathbf{I} + \sigma_s) : \nabla \mathbf{v} - \nabla \cdot \mathbf{q}_s \\ &\quad - 3\beta T - \gamma. \end{aligned} \quad (24)$$

## 2.4 Constitutive equations CM

### Kinetic theory

- Analytical theory in molecular dynamics;
- Chapman & Cowling (textbook 1970): the probability distribution functions of the locations and velocities of particles satisfy the Boltzmann equation;
- Chapman-Enskog expansion: expands the pdf around an equilibrium distribution;
- Theory was verified by hard-sphere DPM and found to be very accurate up to  $\alpha_s = 0.3$  (Alder & Wainwright 1960; 1970).
- Limitations when applied to gas-solid flow:
  - 1 Elastic collisions assumed;
  - 2 Isotropy assumed;
  - 3 Gas-solid interaction is not in the analytical theory.

## Kinetic theory of granular flow (KTGF)

- The first limitation has been resolved by the inclusion of a normal restitution coefficient (no tangential friction yet).
- Lun et al 1984; Gidaspow 1994; van der Hoef et al 2006.
- Solids stresses become:

$$\rho_s = \left(1 + 2(1 + e_r)\alpha_s g_0\right) \rho_s \alpha_s T, \quad (25)$$

$$\tau_{s,ij} = \lambda_s (\nabla \cdot \mathbf{v}) \delta_{ij} + \mu_s \left( \frac{\partial v_i}{\partial x_j} + \frac{\partial v_j}{\partial x_i} - \frac{2}{3} (\nabla \cdot \mathbf{v}) \delta_{ij} \right) \quad (26)$$

- Collision dissipation in  $T$ -equation:

$$\gamma = 3(1 - e_r^2) g_0 \rho_s \alpha_s^2 T \left( \frac{4}{d} \sqrt{T/\pi} - \nabla \cdot \mathbf{v} \right) \quad (27)$$

- Beautiful theory; but is it applicable to practical gas-solid flows? Both anisotropy and tangential friction can be important then. Validations in sections 3 and 4.

## 3. Dilute flows

### Simulations of turbulent particle-laden pipe flow using hard-sphere DPM

- 3.1 Setup and comparison with experiments;
- 3.2 Turbulence attenuation and its explanation;
- 3.3 Eulerian stresses and validation of CM;
- 3.4 Sensitivity to simulation parameters (including streamwise length of the computational domain) and the models in DPM;

Results and analysis in this section: Vreman, JFM 2007.

Acknowledgement: To program the hard-sphere collision software module, I studied a piece of code developed by Kuipers et al. (Hoomans et al, Chem. Eng. Sci. 1996) and used in a previous project on channel flow in 2003 (Vreman, Geurts, Deen, Kuipers Kuerten).

## 3.1 Setup and comparison with experiments

### Experiments

- Experiments have been performed by Caraman, Borée & Simonin (PF 2003) and Borée & Caraman (PF 2005).
- Vertical air-solid pipe flow; downward;  $D = 2\text{cm}$ ;  $U_0 = 4\text{m/s}$ .  $Re_\tau = 140$ ; Glass-beads of  $d_p = 60\mu\text{m}$  and  $90\mu\text{m}$ .
- Experimental mass load values ( $m = \alpha\rho_p/\rho_g$ ) are 0.11 and 1.10. This corresponds to  $\alpha = \alpha_s = 5 \cdot 10^{-5}$  and  $5 \cdot 10^{-4}$ .

### Simulations

- Pipe section with periodic boundaries;  $L_z = 5D$  or  $10D$ .
- Kolmogorov scale  $\eta = 0.14\text{mm} > d_p$ . Hence volume of the smallest grid cell is  $\gg$  particle volume.
- DNS of air-phase (with drag law); Cases:  $0.11 \leq m \leq 30$ .

## Lowest mass load simulation; $\alpha = 5 \cdot 10^{-5}$

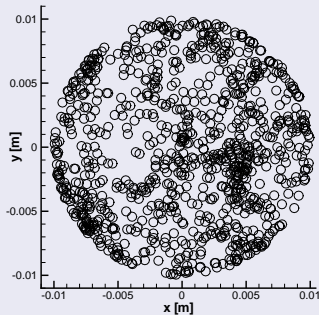
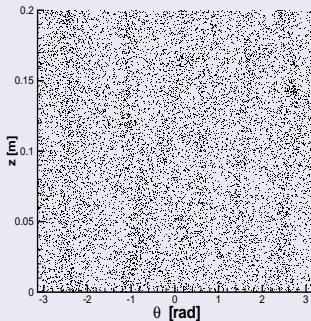


**Figure:** Snapshots of particles in several slices of the domain. Planes shown are at  $r = 0.97\text{cm}$  and  $z = 10\text{cm}$ .

## Highest mass load simulation; $\alpha = 0.015$ ; $1.2 \cdot 10^6$ particles

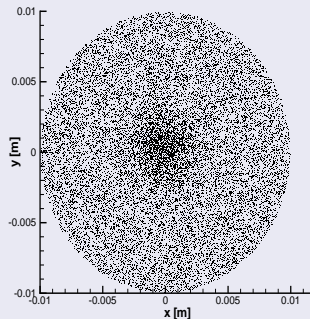
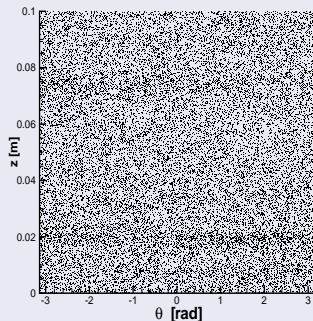


**Figure:** Snapshots of particles in several slices of the domain. The planes shown are at  $r = 0.12\text{cm}$  (a) and  $z = 2\text{cm}$ . M1 M2 M3

## Simulation results (continued)

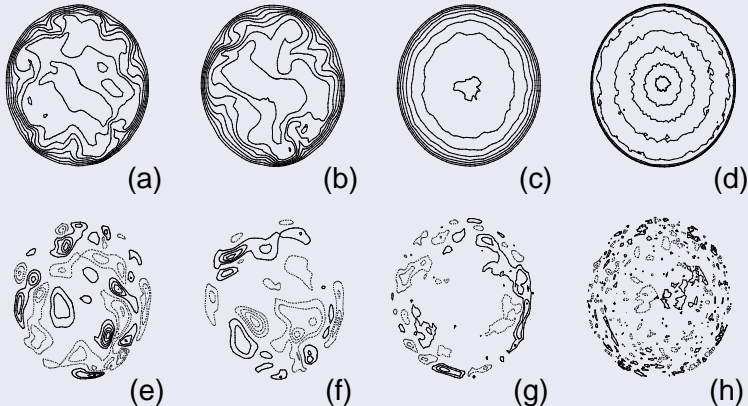
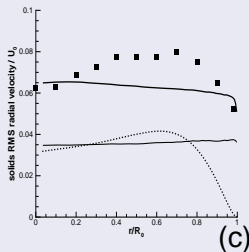
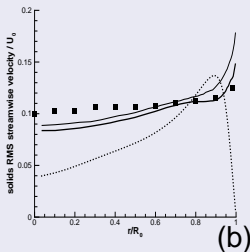
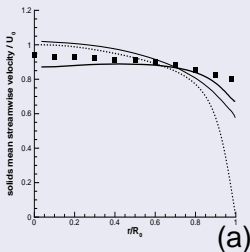


**Figure:** Snapshots of  $u_z$  (top) and  $u_\theta$  (bottom) for four cases, from left to right:  $m = 0, 0.23, 1.1$  and  $30$ . Contour increments are  $0.5$  (a-d),  $0.1$  (ef), and  $0.02$  (gh). Negative contours are dashed. M4 M5 M6

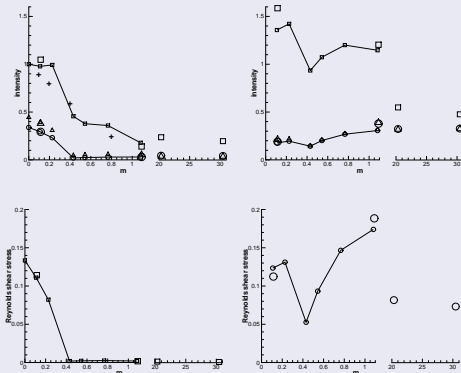
## Comparison with experiments: $m = 1.1$ and $d_p = 90\mu\text{m}$ .



- Particle velocity profiles: mean (a), streamwise intensity (b), radial intensity (c). Simulations without (thin solid) and with wall-roughness model (thick solid). Dotted: unladen. Symbols: experimental data Borée & Caraman (2005).
- Wall roughness model: random perturbation of the collision normal vector at the wall with 20% (a variation on Sommerfeld 1992). **Wall roughness is important.**

## 3.2 Turbulence attenuation and its explanation

Turbulence attenuation; all cross-sectionally averaged Reynolds stresses from the simulations



LEFT: air  
RIGHT: solids

TOP: intensities;  
(+: experiments  
Kulick *et al.* 1994)  
BOTTOM: shear  
stresses

## Explanation of turbulence attenuation

- Turbulence attenuation induced by particles is a classic problem. It is called the Toms effect when the particles are polymers.
- The attenuation is often attributed to extra dissipation that would be caused by the particle motion, since attenuation is also observed in isotropic particle-laden turbulence (Hwang & Eaton 2006).
- Footnote Owen (1969): “In a statistically steady flow, an increasing portion of the shear stress developed in the gas is transferred to the particles, in the form of a momentum flux, as the wall is approached”
- Thus: conservation of momentum is important (has also been remarked by Mito & Hanratty 2006).

## Equation for the turbulent production

- Neglect the friction of particle collisions:

$$\frac{\rho_g}{r} \frac{\partial}{\partial r} \left( r(\overline{u_r u_z} + \overline{u'_r u'_z}) \right) = \rho_g g + \rho_g a_{\text{ext}} + \frac{1}{1 - \alpha_0} \overline{f_z} + \nu \frac{\rho_g}{r} \frac{\partial}{\partial r} \left( r \frac{\partial \overline{u_z}}{\partial r} \right), \quad (28)$$

$$\frac{\rho_s}{r} \frac{\partial}{\partial r} \left( r \overline{\alpha} (\widetilde{v_r v_z} + \widetilde{v'_r v'_z}) \right) = \overline{\alpha} \rho_g g - \overline{f_z}. \quad (29)$$

- Summation:

$$\frac{1}{r} \frac{\partial}{\partial r} (r \overline{u'_r u'_z}) = -\frac{m}{r} \frac{\partial}{\partial r} (r \widetilde{v'_r v'_z}) - mb + (1+m)g + a_{\text{ext}} + \frac{\nu}{r} \frac{\partial}{\partial r} \left( r \frac{\partial \overline{u_z}}{\partial r} \right)$$

- Substitute global force balance:

$$(1+m)g_z + a_{\text{ext}} = 2 \frac{\tau_w}{\rho_g R_0} = 2 \frac{u_\tau^2}{R_0}, \quad (30)$$

## Equation for the turbulent production (continued)

$$P^g = \frac{2m}{R_0^2} \int_0^{R_0} \widetilde{v_r'' v_z''} \frac{\partial \bar{u}_z}{\partial r} r dr - bm + \frac{4u_\tau^2}{R_0^3} \int_0^{R_0} \bar{u}_z r dr - \frac{2\nu}{R_0^2} \int_0^{R_0} \left( \frac{\partial \bar{u}_z}{\partial r} \right)^2 r dr$$

- Results show that  $\bar{u}_z$  is not affected by  $m$  to leading order. Thus:

$$\frac{P^g}{P_0^g} = 1 - m \frac{B - \frac{2}{R_0^2} \int_0^{R_0} \widetilde{v_r'' v_z''} \frac{\partial \bar{u}_z}{\partial r} r dr}{P_0^g} + O(m^2). \quad (31)$$

- If  $\alpha$  is uniform ( $B = 0$ ) and  $\widetilde{v_r'' v_z''} = \overline{u_r' u_z'}$  then  $\frac{P^g}{P_0^g} \approx 1 - m$ .

## Integrated RANS budgets: air

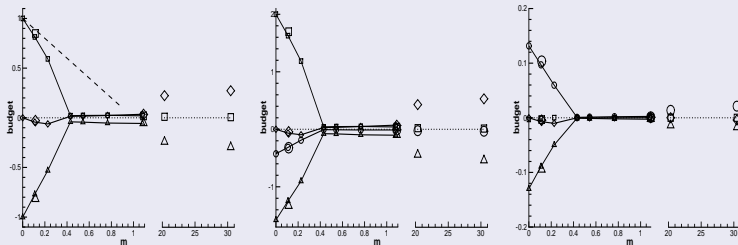


**Figure:** Budgets  $k$ -eqn,  $R_{zz}$ -eqn and  $R_{rr}$ -eqn.

- 1 –  $m$  tendency confirmed;
- small dissipation due to particles;
- pressure strain shows larger relative reduction than turbulent production and turbulent dissipation.

## Turbulence attenuation in simplified systems (no DPM)

$$\nabla \cdot \mathbf{u} = 0, \quad (32)$$

$$\rho_g \left( \frac{\partial \mathbf{u}}{\partial t} + \mathbf{u} \cdot \nabla \mathbf{u} \right) = -\nabla p + \rho_g \nu \nabla^2 \mathbf{u} + (\rho_g \mathbf{g} + \mathbf{a}_{ext}) \mathbf{e}_z + \mathbf{f}_i,$$

Three options for the source term are considered:

- 1 Only effect of mean velocity difference:

$$\mathbf{f}_1 = -c(\bar{\mathbf{u}} - \mathbf{v}_0), \quad c = m\rho_g/\tau_p. \quad (33)$$

- 2 Only effect of additional dissipation in TKE:

$$\mathbf{f}_2 = -c(\mathbf{u} - \bar{\mathbf{u}}). \quad (34)$$

- 3 Previous options combined:

$$\mathbf{f}_3 = \mathbf{f}_1 + \mathbf{f}_2 = -c(\mathbf{u} - \mathbf{v}_0). \quad (35)$$

## Simplified systems: results and conclusions

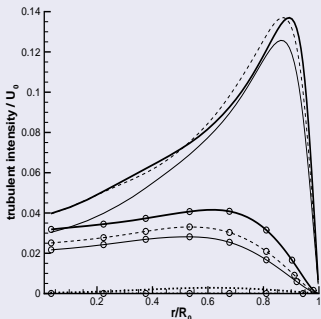


**Figure:** Streamwise and radial (marker) turbulent intensities: no forcing term (thick solid), and  $f_1$  (thin solid),  $f_2$  (dashed),  $f_3$  (dotted).

- In all three cases attenuation. Thus two causes! **Both the nonuniform mean velocity difference and the dissipation by particles play a role!**
- Why is the mean velocity difference nonuniform? Because solids mean velocity profile is more horizontal than air mean velocity profile. And why? Because

- 1 particles slip at the wall;
- 2 particles collide;
- 3 particles slowly respond to air;

## 3.3 Eulerian stresses and validation of CM

### Integrated RANS budgets: solids

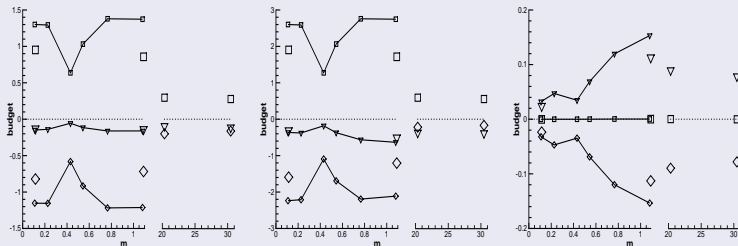


**Figure:** Budgets  $k_s$ -eqn,  $R_{zz}^s$ -eqn and  $R_{rr}^s$ -eqn.

$T = \frac{2}{3}k_s$ ; the kinetic theory CM incorrectly predicts collisional dissipation  $\gamma$  (triangles): model is 10 times too low at  $m = 1.1$ . Probably due to anisotropy and/or frictional dissipation.

## 3.4 Sensitivity to parameters and models in DPM

### Variations for $m = 1.1$ and $d_p = 90\mu\text{m}$

|    | Description         | $2k^g/l_0$ | $2k^s/l_0$ | $R_{zz}^s/l_0$ | $P^s/P_0$ |
|----|---------------------|------------|------------|----------------|-----------|
| 1  | standard S90f       | 0.029      | 1.69       | 1.40           | 0.84      |
| 2  | lift force          | 0.025      | 1.69       | 1.40           | 0.84      |
| 3  | grid G1             | 0.002      | 1.66       | 1.38           | 0.86      |
| 4  | grid G2             | 0.020      | 1.65       | 1.37           | 0.84      |
| 5  | $L_z = 10D$         | 0.021      | 1.66       | 1.37           | 0.84      |
| 6  | bidispersed         | 0.021      | 1.71       | 1.44           | 0.90      |
| 7  | inter-particle drag | 0.019      | 1.58       | 1.32           | 0.81      |
| 8  | interpolation J1    | 0.019      | 1.66       | 1.38           | 0.85      |
| 9  | $\mu_w = 0.5$       | 0.019      | 1.80       | 1.47           | 0.94      |
| 10 | $\mu = 0.3$         | 0.019      | 1.65       | 1.40           | 0.86      |
| 11 | $e_r = 0.99$        | 0.019      | 1.69       | 1.40           | 0.86      |
| 12 | $\beta_0 = 0$       | 0.019      | 1.67       | 1.39           | 0.85      |

## Length of domain matters & physical length-scales

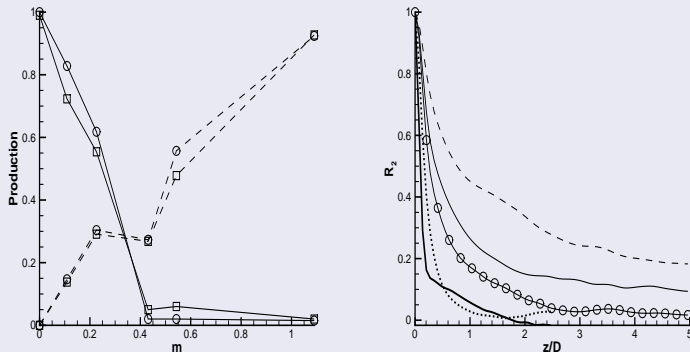


**Figure:** LEFT: air production term  $P^g$  (solid lines) and solids production term  $\rho_p \alpha_0 P^s / (\rho_g (1 - \alpha_0) P_0) \approx m P^s / P_0$  (dashed lines) for simulations with length  $10D$  (circles) and  $5D$  (squares). RIGHT: Two-point correlation function  $R_2(z)$  for  $m = 0$  (circles),  $0.11$  (solid),  $0.23$  (dashed),  $1.1$  (dotted) and  $30$  (thick solid).

## Length of domain & physical length-scales (continued)

| $m$  | $\lambda/D$ | $\lambda_{St}$ | $c_i$ [ $10^6/s$ ] | $c_w$ [ $10^6/s$ ] | $\lambda_f/D$ | $\lambda_{f,M}/D$ |
|------|-------------|----------------|--------------------|--------------------|---------------|-------------------|
| 0    | 0.8         | -              | -                  | -                  | -             | -                 |
| 0.11 | 1.4         | 3.2            | 0.20               | 0.14               | 13            | 27                |
| 0.23 | 4.0         | 3.5            | 0.48               | 0.14               | 10            | 13                |
| 1.10 | 0.35        | 10             | 0.89               | 0.43               | 5             | 4                 |
| 30   | 0.15        | 10             | 215                | 12.3               | 0.5           | 0.14              |

**Table:** Length-scales and collision numbers. MOVm0.23 MOVm30

- 1  $\lambda$ : turbulence length-scale based on  $R_2 \approx 0.2$ .
- 2  $\lambda_{St} = V_z \tau_p$ : Stokes response path length.
- 3  $\lambda_f = V_z N_{part} / (2c_i + c_w)$ : free path length (distance travelled between two collisions); compared with Maxwellian prediction  $\lambda_{f,M}$  (isotropic).

## 4. Dense flows

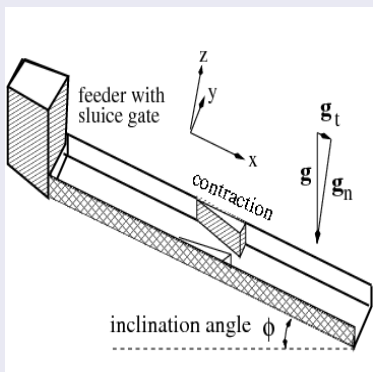
### Granular flow through a contraction simulated with soft-sphere DPM. Contents:

- 4.1 Laboratory experiments (movies) and classification of flow regimes.
- 4.2 New physical explanation for the reservoir formation in granular flow on an inclined plane through a contraction.
- 4.3 Comparison with soft-sphere DPM simulation.
- 4.4 Validation of continuum models using DPM database.

Results and analysis are taken from *A.W. Vreman, M. Al-Tarazi, J.A.M. Kuipers, M. van Sint Annaland, O. Bokhove, JFM 2007* (Bokhove was originator and supervisor of this project; he was inspired by the geological formation of the bed of the Rhine; the measurements were carried out on the site of the University of Twente).

## 4.1 Experiments and classification of flow regimes

Experimental setup:



- Aluminium chute: 2m  $\times$  0.13m;
- Inclination:  $\tan \phi \approx 0.35$ ;
- Without contraction almost uniform flow (gravity and friction balance);
- Fluid material:
  - 1 Glass-beads: 0.3mm, 0.6mm, 1mm (spherical);
  - 2 Poppy seeds (non-spherical).

## Classification of flow regimes

Four flow regimes  
(movies show the  
'hydraulic' jumps):

- I supercritical flow
- II unsteady lake outside contraction
- III steady reservoir inside contraction
- IV hysteresis (multiple states)

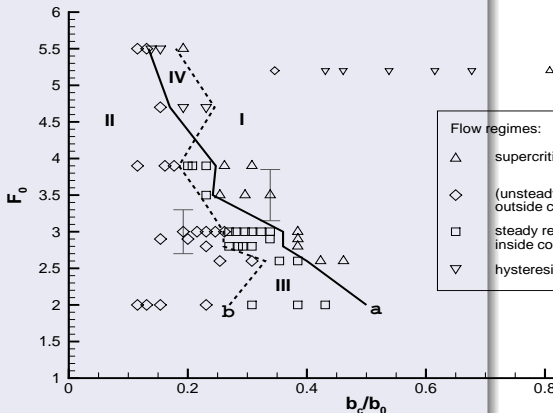


**Figure:** Upstream Froude number  $F_0 = u_0/\sqrt{gh_0}$  against nozzle width  $b_c$ .

## 4.2 Explanation for reservoir formation

- The reservoir regime is interesting:
  - because of the geological example;
  - because classical hydraulic theory can not predict this. reservoir.
- Averaged equations in 1D:

$$\frac{\partial \alpha b h}{\partial t} + \frac{\partial \alpha b h u}{\partial x} = 0, \quad (36)$$

$$\frac{\partial u}{\partial t} + \frac{\partial (u^2/2)}{\partial x} = a g_n - g_n \frac{\partial h}{\partial x}, \quad (37)$$

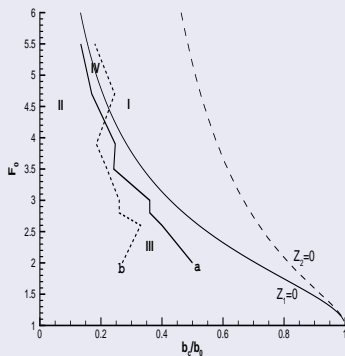
$$a = \tan(\phi) - \mu. \quad (38)$$

- The (dynamic) friction coefficient  $\mu$  is unknown. Coulomb closure (1770?):  $\mu$  is constant.

## Application of classical hydraulic theory

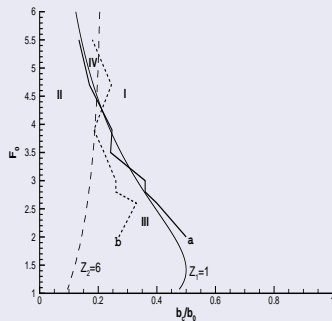
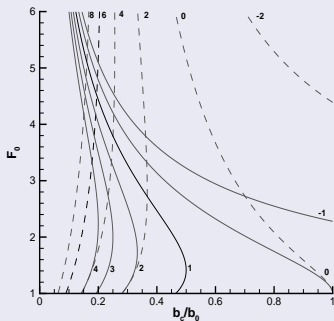
Shapiro 1953; Baines & Whitehead 2003; Akers & Bokhove 2006.

- Analysis:
  - Inviscid (gravity cancels against friction:  $a = 0$ );
  - $F = 1$  at the nozzle: thin solid line;
  - Hydraulic jump (shock wave) at contraction entrance: thin dashed line.
- Thin lines span only three regimes: **no steady reservoir!**



## Extended theory (acceleration integrals)

- Repeat the analysis with  $a \neq 0$ :  $A = \int_0^X adx$ ;  $Z = \Delta A/h_0$ .
- For nonzero  $Z$  the lines shift and regime III emerges.
- Conclusion: **the reservoir is a frictional effect!**



- To learn more about friction: DPM simulation (upcoming).

### 4.3 Soft-sphere DPM simulation: results

- Reservoir case: 1mm spheres (380000);
- Model:  $\mu_{t,DPM} = \tan(\phi) = 0.344$ ,  $e_r = 0.97$ ,  $k_n = 100\text{N/m}$ ;
- drag neglected, 10 seconds, Runge Kutta 4.

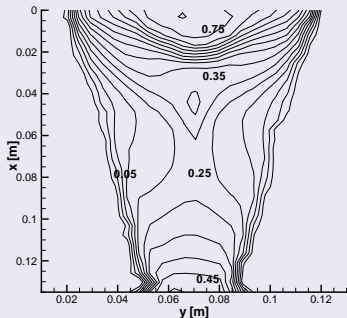


**Figure:** Measured top streamwise velocity (Particle Image Velocimetry). MOVIE.

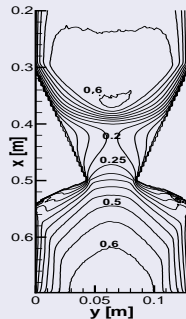


**Figure:** Depth-averaged streamwise velocity (simulation). MOVIE.



## Reservoir case: simulation results.

$h$ : consider all particles in  $2 \times 2\text{mm}^2$  square column:

$$h(x, y, t) = \hat{z} + \frac{1}{2}d + \sqrt{\widehat{z^2} - \hat{z}^2}, \quad \hat{z}(x, y, t) = \frac{1}{\tau} \int_{t-\tau}^t \max_i \{z_i\} dt,$$

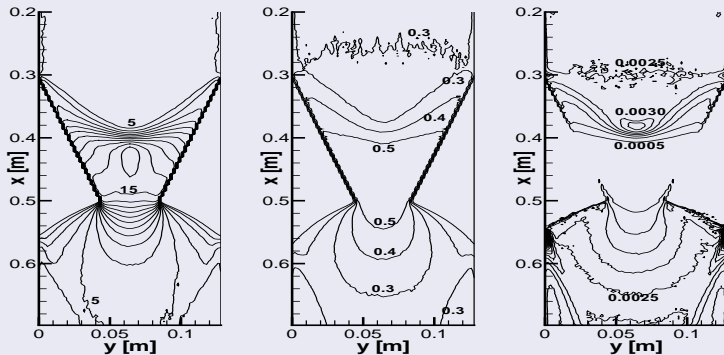


**Figure:** Steady state depth  $h$  and depth-averaged  $\alpha$  and  $T$ . Contour increments: 1mm, 0.1,  $0.0005\text{m}^2/\text{s}^2$ .

## Simulations for four nozzle widths (1D statistics)

| $b_c$ | curve       | time (s) | # of particles |
|-------|-------------|----------|----------------|
| 130mm | dashed      | 7.0      | 284000         |
| 70mm  | dotted      | 6.3      | 304000         |
| 50mm  | dash-dotted | 7.6      | 323000         |
| 40mm  | solid       | 10.8     | 378000         |

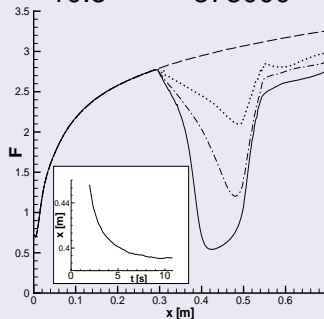
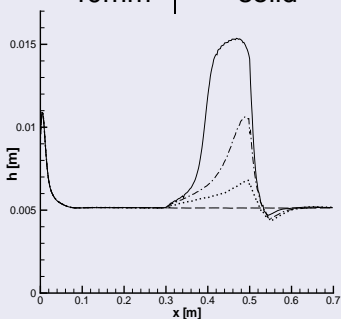
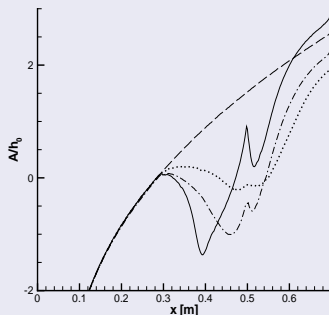
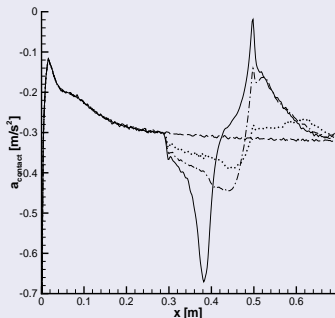


**Figure:** Depth (left) and Froude (right). Reservoir case (solid) becomes subcritical in reservoir! ( $F < 1$ ).

## Four nozzle widths (continued)

- LEFT:  $a_{contact}$  (contact forces normalized with  $\rho g h$ ).
- RIGHT:  $A = \int_0^x a dx$ ;  $a = \tan\phi + a_{contact} + dh/dx$ .
- $A$  increases strongly in the reservoir! Indeed  $Z \approx 2$ !

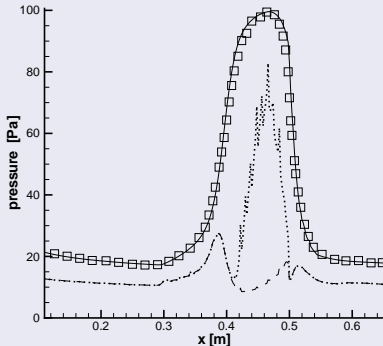


## 4.4 Validation of continuum models using DPM database (reservoir case)

Frictional-kinetic models (Lun et al 1984; Johnson et al 1990)

$$\sigma_{\mathbf{c}} \approx -\left(\rho_p \alpha T(1 + 4\alpha g_0) - \mu_b \nabla \cdot \mathbf{u}\right) \mathbf{I} + 1.2\mu_b \mathbf{S},$$

$$\rho_{mod} = \rho_p \alpha T(1 + 4\alpha g_0) - \mu_b \nabla \cdot \mathbf{u} + N_f(\alpha).$$



Depth-average pressure.

The simulation pressure,  $\frac{1}{2}\rho_{wall}$  ( $\square$ ), validates the

- 1 'hydrostatic' pressure  $\frac{1}{2}\rho_p \alpha g_n h$  (solid);
- 2  $\rho_{mod}$  with (dotted) and without frictional term  $N_f$  (dashed).

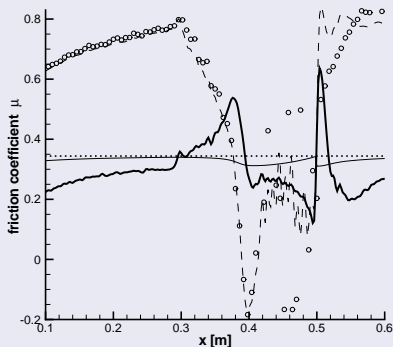
## Validation of continuum models for $\mu$

*Thick solid:* 'True' friction  $\mu = -a_{\text{contact}} - dh/dx$ .

Friction is low in reservoir, but high in shock before reservoir.

Continuum models:

- Coulomb (*dotted*);
- Frictional-kinetic model in 1D (*dashed*) and 2D (*circles*); includes a bottom shear stress model by Hui et al (1984) (boundary condition!);
- Empirical Savage & Hutter model (*thin solid*)  
 $\mu = 0.344(1 - e^{-0.64F})$ .



## 5. Mathematics of continuum models

### Well-posedness of the equations

**5.1** Ill-posedness implies instabilities with infinite growthrate!

**5.2** The most simple two-fluid system is ill-posed.

**5.3** Generalization of the interaction force (drag-law) to a positive definite operator.

**5.4** Then the simple two-fluid system becomes well-posed.

**5.5** Generalization to fluids with  $N$  components.

Sections 5.3-5 are based on Vreman, Physica D (2007).

## 5.1 Ill-posedness & infinite growthrate

- Linear vector equation

$$A \frac{\partial \mathbf{y}}{\partial t} + B \frac{\partial \mathbf{y}}{\partial x} = D \mathbf{y} \quad (39)$$

with constant coefficient matrices  $A$ ,  $B$  and  $D$ .

- Search for a solution  $\mathbf{y} = \hat{\mathbf{y}} e^{kx - \omega t}$  with  $k$  real and  $\omega$  complex.  $Im(\omega)$  is the growthrate and  $Im(\omega) > 0$  implies instability. Substitution gives:

$$\left(-\frac{\omega}{k} A + B - \frac{1}{k} D\right) \hat{\mathbf{y}} = 0 \quad (40)$$

- Define  $\lambda = \omega/k$  and let  $k \rightarrow \infty$ . Then the algebraic term  $(D\hat{\mathbf{y}})$  plays no role:

$$(\lambda A - B) \hat{\mathbf{y}} = 0 \quad (41)$$

### Ill-posedness & infinite growthrate (continued)

- Eq. (41) has a non-trivial solution  $\hat{\mathbf{y}}$  if

$$P(\lambda) = \det(\lambda A - B) = 0. \quad (42)$$

- $\lambda$  is a generalized eigenvalue ('characteristic velocity').
- Growthrate  $Im(\lambda)k \rightarrow \infty$  if  $Im(\lambda) > 0$ .
- Therefore only  $Im(\lambda) \leq 0$  is physical.
- However, the characteristic polynomial  $P(\lambda)$  has real coefficients, such that all complex roots occur as complex conjugate pairs.
- Thus all roots (characteristic velocities) should be **real**.
- Complex roots: the problem is ill-posed in the sense of Hadamard; the solution does not depend *continuously* on the initial data. Real roots: the problem is well-posed.

## 5.2 Ill-posedness of the most simple two-fluid system

- Classic analysis: Anderson & Jackson (1963; 1968), Pigford & Baron (1965), Ramshaw & Trapp (1978), Drew & Passman (1998), Prosperetti & Tryggvason (2007).
- Incompressible inviscid two-fluid equations with standard drag in 1D:

$$\begin{aligned} \frac{\partial \alpha}{\partial t} + \frac{\partial \alpha u_1}{\partial x} &= 0, \\ \frac{\partial (1-\alpha)}{\partial t} + \frac{\partial (1-\alpha) u_2}{\partial x} &= 0, \\ \alpha \rho_1 \frac{\partial u_1}{\partial t} + \alpha \rho_1 u_1 \frac{\partial u_1}{\partial x} &= \alpha \frac{\partial p}{\partial x} - c(u_1 - u_2), \\ (1-\alpha) \rho_2 \frac{\partial u_2}{\partial t} + (1-\alpha) \rho_2 u_2 \frac{\partial u_2}{\partial x} &= (1-\alpha) \frac{\partial p}{\partial x} - c(u_2 - u_1). \end{aligned}$$

## Calculation of characteristic velocities

- Linearization around constant field (uniform flow):  
 $u_i \rightarrow u_i + u'_i$ .
- Variable vector  $\mathbf{y} = [\alpha' \ u'_1 \ u'_2 \ \rho']^T$
- Characteristic equation:

$$\begin{vmatrix} \lambda - u_1 & -\alpha & 0 & 0 \\ \lambda - u_2 & 0 & (1-\alpha) & 0 \\ 0 & \rho_1(\lambda - u_1) & 0 & -1 \\ 0 & 0 & \rho_2(\lambda - u_2) & -1 \end{vmatrix} = 0.$$



$$\lambda = \frac{\alpha\rho_2 u_2 + (1-\alpha)\rho_1 u_1 \pm i|u_1 - u_2|\sqrt{\alpha(1-\alpha)\rho_1\rho_2}}{\alpha\rho_2 + (1-\alpha)\rho_1}$$

- Characteristic velocities are not real if  $u_1 \neq u_2$ .

## 5.3 Generalization of the drag-interaction force

- No complex roots occur if we add a surface tension term (Ramshaw & Trapp 1978) or if we add standard viscous terms (Arai 1980).
- However, these are not general solutions since surface tension is not always important. Viscosity is not always important either, except from the boundary layers around particles, *but these are not macroscopic and should only be represented by the drag force!*
- Therefore Vreman (2007) proposed to extend the drag law with velocity derivatives to obtain real roots:
  - 1 Express interaction force in a positive definite operator  $C$ :

$$f_{ij} = -C(u_i - u_j), \quad \text{for example } C = cI - \nabla \cdot (a\nabla), \quad a, c > 0.$$

- 2 Third law of Newton is satisfied:  $f_{21} = -f_{12}$ .
- 3 Total kinetic energy always decreases (entropy law holds).

## 5.4 Well-posedness of the two-fluid system with generalized drag in 1D

- The right-hand sides of the two momentum equations in section 5.2 are extended:

$$\begin{aligned}\dots &= \dots + \frac{\partial}{\partial x} \left( a \frac{\partial(u_1 - u_2)}{\partial x} \right), \\ \dots &= \dots - \frac{\partial}{\partial x} \left( a \frac{\partial(u_1 - u_2)}{\partial x} \right).\end{aligned}$$

- An extra variable and an extra equation is added to get rid of the second-order derivatives:

$$\tau = \frac{\partial(u_1 - u_2)}{\partial x}.$$

## Well-posedness generalized drag in 1D (continued)

- Characteristic equation:

$$\begin{vmatrix} \lambda - u_1 & -\alpha & 0 & 0 & 0 \\ \lambda - u_2 & 0 & (1-\alpha) & 0 & 0 \\ 0 & \rho_1(\lambda - u_1) & 0 & -1 & a \\ 0 & 0 & \rho_2(\lambda - u_2) & -1 & -a \\ 0 & 0 & 1 & -1 & 0 \end{vmatrix} = 0.$$

- Only one root, but it is real:  $\lambda = (1-\alpha)u_1 + \alpha u_2$ .
- The generalization of the drag law leads to a partially parabolic system; the number eigenvalues has reduced with one.
- Although the dimension of the system is five, two eigenvalues disappear because of the parabolization, the other two disappear because of the infinite speed of sound in incompressible flow.

## 5.5 Generalization to fluids with $N$ components

- Drag in momentum equation  $i$ :  $-\sum_{j=1}^N C_{ij}(u_i - u_j)$ .
- The  $\frac{1}{2}N(N + 1)$  positive definite operators  $C_{ij}$  model the interaction forces between components  $i$  and  $j$ .
- The pressure terms become  $\alpha_i \nabla p$ .
- Consider 1D incompressible flow.
- The dimension of the system is  $2N$  with standard drag.
- Generalized drag with second order derivatives,

$$C_{ij} = c_{ij}I - \nabla \cdot \mathbf{a}_{ij} \nabla (u_i - u_j),$$

leads to  $N - 1$  characteristic velocities.

- Are the characteristic velocities real? (Is the system well-posed?)

## Generalization to fluids with $N$ components (continued)

- Characteristic equation:

$$\begin{vmatrix} \lambda - u_1 & 0 & \dots & -\alpha_1 \\ 0 & \lambda - u_2 & \dots & -\alpha_2 \\ \vdots & \vdots & \ddots & \vdots \\ u_N - \lambda & u_N - \lambda & \dots & -\alpha_N \end{vmatrix} = 0. \quad (43)$$

- This reduces to:

$$Q(\lambda) = \sum_i (\alpha_i \prod_{j \neq i} (\lambda - u_j)) = 0, \quad \sum_i \alpha_i = 1.$$

- Conjecture: **all roots of  $Q(\lambda)$  are real:**

- 1 this has been proven analytically for  $N = 2$  and  $N = 3$ ;
- 2 no counter-example was found when random numerical values for  $\alpha_i$  and  $u_i$  were tried for  $N \geq 4$ ;
- 3 *the mathematical proof for  $N \geq 4$  is still an open problem!*